RSC Advances

ROYAL SOCIETY OF CHEMISTRY

www.rsc.org/advances

Structural Evolution, Sequential Oxidation and Chemical Bonding in Tri-yttrium Oxide Clusters: $Y_3O_x^-$ and Y_3O_x (x = 0–6)

Lei Xu[a], Chan-Juan Xia[a], Ling-Fei Wang[a], Lu Xie[a], Bin Wang[a], Yong-Fan Zhang[a,b]*, Xin Huang [a,b]*

[a]*College of Chemistry, Fuzhou University, Fuzhou, Fujian 350116, PR China*
[b]*Fujian Provincial Key Laboratory of Theoretical and Computational Chemistry, Xiamen, Fujian 361005, PR China*

*Corresponding author. Tel.: +86 591 22866139; fax: +86 591 22866156.
E-mail address: zhangyf@fzu.edu.cn (Y. -F. Zhang); xhuang@fzu.edu.cn (X. Huang)

Abstract

We report a systematic and comprehensive investigation on the electronic structures and chemical bonding of a series of tri-yttrium oxide clusters, $Y_3O_x^{-/0}$ (x = 0–6), using density functional theory (DFT) calculations. Generalized Koopmans' theorem is applied to predict the vertical detachment energies (VDEs) and simulate the photoelectron spectra (PES) for $Y_3O_x^-$ (x = 0–6) clusters. A trend of sequential oxidation is observed from Y_3O^- to $Y_3O_6^-$. All of these clusters tend to form the structures with a capped oxygen atom. For $Y_3O_x^{-/0}$ (x = 2–4), the O atoms are shown to prefer the bridging sites of $Y_3O^{-/0}$, whereas the fifth O atoms for $Y_3O_5^{-/0}$ are bonded to the terminal sites. As for the oxygen-rich clusters $Y_3O_6^-$ and Y_3O_6, O_2^{2-} and $O_2^{-\bullet}$ units occur which can be regarded as the products reduced dioxygen by $Y_3O_4^-$ and Y_3O_4, respectively. σ- and π-aromaticity is found in Y_3^- by molecular orbital analysis and Adaptive Natural Density Partitioning (AdNDP) analysis. Molecular orbital analyses are performed to analyze the chemical bonding in the tri-yttrium oxide clusters and to elucidate their electronic and structural evolution.

Keywords: Yttrium oxide cluster; Density functional calculation; Electronic structures; Simulated photoelectron spectroscopy; Aromaticity; Molecular orbital

1. Introduction

Yttrium oxides have important applications in the field of catalysts, fireproofing, electrode materials, magnetic materials and so forth[1–11], especially used as doping agents for catalyst supports and catalysts[8–11]. For instance, yttria-doped alumina is more thermally stable than bare alumina and can be used as the catalyst support for the thermo-catalytic cracking process[8,9]. Furthermore, the homonuclear yttrium oxide clusters and heteronuclear aluminum-doped yttrium oxide clusters have exhibited different catalytic performances in redox reactions with N_2O/CO. The yttrium oxide cluster doped with aluminum ($YAlO_3^{+\bullet}$) was proved to bring about efficient CO oxidation and the reaction pattern of $YAlO_3^{+\bullet}$ is quite different from that of $Y_2O_3^{+\bullet}$ as a result of the doping effects.[10] As a first step in developing a comprehensive understanding of complex catalytic processes on early transition-metal oxides, we are interested in systematically studying the electronic structure and chemical bonding of isolated transition-metal oxide clusters.

Yttrium oxide clusters have been studied both experimentally[10, 12 – 14] and theoretically[10,11,15–18]. The photoionization spectra of yttrium clusters Y_n and Y_nO (n = 2–31) have been recorded by Knickelbei and a steep nonmonotonic decrease of ionization potentials (IPs) is discovered up to about ten atoms followed by a more gradual decline[12]. Wu and Wang[13] have reported the photoelectron spectrum and electronic structures of YO_n^- (n = 1–5). Pramann and co-workers[14] obtained the photoelectron spectrum of Y_nO_m (n = 2–10, m = 1–3) in which a shifting of threshold energies to higher binding energies was observed with the increase of the cluster size n. Recently, attentions have also been focused on theoretical studies of the yttrium oxide clusters. For example, the structural and electronic properties of Y_3O and Y_4O were studied by Gu et al, where the structures of Y_3O and Y_4O were found to be pyramid and bi-pyramids, respectively and the calculated electron affinities and ionization potentials were in good agreement with the available experimental data[15,16]. In addition, Yang and co-workers investigated the structural, electronic, and magnetic

properties of Y_nO (n = 2–14)[17]. The calculated ionization potentials and electron affinities were in good agreement with the experimental results implying that the ground states of these clusters are reliable to better understand the yttrium oxide clusters and materials. Very recently, Rahane et al[18] reported a DFT study on the structural and electronic properties of $(Y_2O_3)_n^{0\pm1}$ (n =1–10) clusters and found that the charge transfer from Y atoms to oxygen atoms increases with the increasing of cluster size. To the best of our knowledge, there is still scarce investigation on tri-yttrium oxide clusters.

We have been interested in developing cluster models to characterize metal cluster species in the gas phase and to provide fundamental mechanistic insights for catalysts[19–24], as well as the novel all-metal aromaticity[25]. In the previous studies, all-metal aromaticity has firstly been reported using Al_4^{2-} as an example with a doubly σ- and π-aromaticity[26]. New computational evidence has been presented about triple (σ-, π- and δ-) aromaticity in the lowest D_{3h} ($^1A_1'$) singlet state of Hf_3[27]. Nowadays, a few review articles concerning all-transition-metal aromaticity/antiaromaticity have been published[28–35]. For example Boldyrev et al[28] performed Adaptive Natural Density Partitioning (AdNDP) method to state the aromaticity for the Sc_3^- (D_{3h} $^1A_1'$) cluster. σ- and π-aromaticity represents a mode of chemical bonding and may play an important role in multinuclear transition metal compounds.

In this work, we focus on exploring the geometric and electronic structures of early transition metal clusters and their oxide clusters. DFT calculations are employed to elucidate the electronic structure and chemical bonding of $Y_3O_x^{-/0}$ (x = 0–6). In particular, the ground states of $Y_3O_6^{-/0}$ are found to be interesting species, which may be viewed as molecular models for dioxygen activation by $Y_3O_4^{-/0}$. A sequential oxidation is observed in the $Y_3O_x^-$ (x = 0–6) clusters as a function of x. The AdNDP method is performed to analyze the aromaticity of Y_3^- cluster, indicating that the Y_3^- possesses σ- and π-aromaticity.

2. Computational Methods

The theoretical calculations were performed at the DFT level using the BP86 functional[36,37]. The global minimum searches were performed using analytical gradients with the Stuttgart relativistic small core basis set and effective core potential [38,39] augmented with two *f*-type and one *g*-type polarization function for yttrium [$\zeta(f)$ = 0.144, 0.546; $\zeta(g)$ = 0.249] as recommended by Martin and Sundermann[40] and the aug-cc-pVTZ basis set[41,42] for oxygen. Scalar relativistic effects, that is, the mass velocity and Darwin effects, were taken into account via the quasi-relativistic pseudo-potentials. Vibrational frequency calculations were performed to verify the nature of the stationary points. The vertical electron detachment energies (VDEs) were calculated using the generalized Koopmans' theorem by adding a correction term to the eigenvalues of the anion[43]. The correction term was calculated as $\delta E = E_1 - E_2 - \varepsilon_{HOMO}$, where E_1 and E_2 are the total energies of the anion and neutral, respectively, in their ground states at the anion equilibrium geometry and ε_{HOMO} corresponds to the eigenvalue of the highest occupied molecular orbital (HOMO) of the anion. The relative energies of the low-lying structures were further evaluated via single-point calculations at the coupled cluster [CCSD(T)] [44 – 48] level with the Y/Stuttgart +2*f*1*g*/O/aug-cc-pVTZ basis sets at the BP86 geometries. For open-shell systems, the UCCSD(T) approach was used, where a restricted open-shell Hartree–Fock (ROHF) calculation was initially performed and the spin constraint was relaxed in the correlation treatment. In addition, more accurate optimizations in CCSD(T) were carried out for some close-lying structures with Y/Stuttgart +2*f*1*g*/O/aug-cc-pVTZ basis sets. All DFT calculations were performed with the Gaussian 09 software package[49] and the CCSD(T) calculations were done using MOLPRO 2010.1 package[50]. Three-dimensional contours of the molecular orbitals were visualized using the VMD software[51]. Different exchange-correlation functionals were tested for accuracy and consistency. The BP86 functional showed superior results in terms of electron binding energies and structures for yttrium oxide clusters. The previous studies on yttrium oxide clusters[52,53] also have indicated that the BP86 calculations can give good consistency with the experimental results and better

overall performance in predicting the molecular properties. Therefore, we used the results with the BP86 functional for our discussion.

The Adaptive Natural Density Partitioning (AdNDP) method has been recently developed by Boldyrev et al[28]. The principles of the method have been described elsewhere[54]. The AdNDP analysis for the ground state of the Y_3^- cluster was performed using DFT at the BP86/lanl2dz level. The results of the AdNDP analysis were visualized using the MOLEKEL 5.4 software[55].

3. Theoretical Results

The optimized ground states and low-lying isomers (within ~ 0.40 eV) at the BP86 level for anionic $Y_3O_x^-$ and neutral Y_3O_x (x = 0–6) are presented in Figure 1–7, respectively. More optimized geometries at higher energies are given as supplementary material (Figures S1–S7). In the following discussion, O_t, O_b and O_c stand for the terminal, bridging and capped oxygen atoms, respectively.

3.1 Y_3^- and Y_3

For the tri-yttrium clusters, four possible atomic arrangements: linear ($C_{\infty v}$ or $D_{\infty h}$), equilateral triangle (D_{3h}), isosceles triangle (C_{2v}), or completely distorted triangle (C_s) were considered. The ground states and the selected low-lying isomers (within ~ 0.40 eV) of tri-yttrium clusters (Y_3^- and Y_3) are listed in Figure 1. Our theoretical results clearly show that the global minimum of Y_3^- is a D_{3h} ($^1A_1'$) structure (Figure 1a), which is in accordance with the previous study by Chi et al[31]. The corresponding triplet (D_{3h}, $^3A_2''$) (Figure 1b) and (D_{3h}, $^3A_1'$) (Figure 1c) are 0.27 eV and 0.34 eV higher in energy, respectively. The low-lying isomer (Figure 1d) with C_{2v} ($^3A_2$) symmetry is 0.34 eV higher above the ground state.

For the neutral Y_3, the ground state is revealed to be D_{3h} ($^2A_1'$) (Figure 1e). The Y–Y bond is slightly longer (~ 0.08 Å) compared to that of the anion (Figure 1a). In the work by Dai et al[56], the structure (D_{3h}, $^2A''$) (Figure 1f) was predicted to be the ground state of Y_3 using the complete-active-space-multiconfiguration self-consistent-field (CAS-MCSCF) method. However, it is 0.10 eV higher in energy

above the D_{3h} ($^2A_1'$) state in our calculation. The corresponding quartet (D_{3h}, $^4A_2''$) (Figure 1g) is 0.27 eV higher in energy at the BP86 level. Similar to the anion, there also exists a C_{2v} ($^4B_2$) structure which is 0.31 eV above the ground state. The single-point CCSD(T) (Table SI) were also carried out, and the results are in agreement with that of our BP86 calculations instead of that of the previous study[56]. Further theoretical calculations with more sophisticated methods may be necessary to resolve the true ground state of Y_3.

3.2 Oxygen-deficient clusters: $Y_3O_x^{-/0}$ (x = 0–4)

3.2.1 Y_3O^- and Y_3O

The optimized ground states and selected low-lying isomers within ~ 0.40 eV for Y_3O^- and Y_3O are presented in Figure 2. The potential energy surfaces for Y_3O^- are rather flat with several closely low-lying isomers near the global minimum. The ground state of Y_3O^- is closed-shell with C_{3v} symmetry (Figure 2a). It can be viewed as a pyramid in which the oxygen atom overtop the plane of tri-yttrium equilateral triangle by 1.092 Å and the bond lengths of Y–O_c and Y–Y are 2.157 Å and 3.142 Å, respectively. The similar corresponding triplet isomer is relaxed to C_s structure (Figure 2c) and was pointed as the global minimum by Gu et al[15], whereas it is revealed to be 0.07 eV higher above the ground state in our calculation at the BP86 level. The second low-lying isomer C_{2v} ($^3B_1$) (Figure 2b) is 0.05 eV above the ground state with a bridging oxygen atom, in which the distances between Y atom and O atoms are 2.002 Å and can be defined as Y–O single bonds[57]. In order to further confirm the ground state of Y_3O^-, CCSD(T) calculations were performed for these close-lying isomers (within ~ 0.20 eV). The results show that the isomer (C_{3v}, $^1A_1$) (Figure 2a) is the global minimum with 0.02 eV more stable than the (C_{2v}, $^3B_1$) structure (Figure 2b) under CCSD(T) optimizations. Other selected low-lying isomers (Figures 2d-2g) are at least 0.20 eV higher at the BP86 level.

The neutral ground state (C_{3v}, $^2A_1$) (Figure 2h) is totally conformed to the result of Yang et al[17], which resembles that of Y_3O^-, except for a slightly lengthened Y–Y bond (by 0.061 Å) and shortened Y–O bond (by 0.016 Å). The low-lying isomer

(Figure 2i) with C_{2v} symmetry is quartet ($^4B_1$), 0.25 eV above the ground state.

3.2.2 $Y_3O_2^-$ and Y_3O_2

To search for the most stable structure of $Y_3O_2^{-/0}$, various structural possibilities with different spin multiplicities are taken into consideration. The potential energy surfaces for $Y_3O_2^-$ and Y_3O_2 are both rather flat. Selected optimized structures of $Y_3O_2^-$ and Y_3O_2, along with their relative energies, are given in Figure 3. The ground state of $Y_3O_2^-$ is a closed-shell (^{1}A') C_s (Figure 3a) configuration with a capped and a bridging O atoms. The similar (C_s, ^{3}A") (Figure3c) and (C_s, ^{3}A') (Figure 3d) isomers in atomic connectivity are 0.18 eV and 0.20 eV higher in energy, respectively. A low-lying (C_s, ^{1}A') (Figure 3b) isomer is located 0.02 eV above the ground state, which possesses two bridging oxygen atoms and its corresponding triplet state (C_{2v}, $^3A_2$) (Figure 3e) is 0.21 eV above the ground state. As for these different structures shown in Figure 2 (within ~ 0.20 eV), further theoretical calculations at the CCSD(T) level are performed to resolve the true global minimum, as reported in Table SI. The CCSD(T) results show that the isomer (C_s, ^{1}A') (Figure 3a) is the ground state, other isomers are at least 0.25 eV higher in energy.

The global minimum (C_s, ^{2}A') (Figure 3h) for the neutral Y_3O_2 is similar to that of $Y_3O_2^-$. The capped oxygen atom is closer to the yttrium atoms at the bottom compared to $Y_3O_2^-$. Three low-lying isomers are found within 0.20 eV at the BP86 level. Similar to the anion, single-point CCSD(T) calculations are performed for these isomers, showing that isomer (C_s, ^{2}A') (Figure 3h) is the ground state. It is lower at least 0.31 eV in energy than others as shown in Table SI.

3.2.3 $Y_3O_3^-$ and Y_3O_3

The low-lying isomers for $Y_3O_3^-$ are given in Figure 4. The ground state (Figure 4a) is a triplet C_s (^{3}A") (Figure 4a) structure and it can be regarded as adding a bridging O atom on the basis of $Y_3O_2^-$. The corresponding singlet state C_s (^{1}A') (Figure 4c) is located 0.32 eV above the ground state. The isomer (C_{3v}, $^3A_1$) (Figure 4b) with three bridging oxygen atoms is only 0.02 eV higher in energy. The Y–O distance is 2.031 Å which can be assigned to be a single bond[57]. The relative energies

for these BP86 geometries (within ~ 0.20 eV) are further calculated using single point CCSD(T) calculations. The results of CCSD(T) calculations (Table SI) are in line with those of DFT calculations and the isomer (C_s, ^{3}A") (Figure 4a) is the most stable structure.

Similar to the anion, the ground state of neutral Y_3O_3 has a capped and two bridging O atoms as shown in Figure 4d (C_s, ^{2}A"). However, the distance between the topmost yttrium atom and the capped oxygen atom is shortened (~ 0.216 Å). The structure (C_s, ^{2}A') (Figure 4f) similar to the (C_s, ^{2}A") (Figure 4d) in geometrical configuration is 0.12 eV less stable. The second low-lying isomer (C_s, ^{2}A') (Figure 4e) with three bridging O atoms is only 0.04 eV higher in energy at the BP86 level which is viewed as the global minimum by Yang et al[58]. The corresponding quartet state (D_{3h}, ^{4}A$_1$') (Figure 4g) is 0.16 eV above the ground state. As for these low-lying isomers, single-point CCSD(T) are calculated using the BP86 results. The isomer in Figure 4d is the most stable structure among the four isomers above-mentioned. Other isomers are no less than 0.12 eV higher in energy as given in supplementary material (Table SI).

3.2.4 $Y_3O_4^-$ and Y_3O_4

We carried out extensive structural searches for the ground states on the potential energy surfaces of $Y_3O_4^{-/0}$ clusters. Three low-lying isomers for $Y_3O_4^-$ clusters within ~ 0.40 eV are found in our calculation. As shown in Figures 5a-5c, they all can be regarded as umbellate clusters with three bridging O atoms and a capped O atom. Single-point CCSD(T) calculations are performed using the BP86 geometries for these three anionic isomers. The results reveal that the ground state is closed shell with C_{3v} (^{1}A$_1$) symmetry (Figure 5a), whereas the corresponding triplet isomers (Figure 5b and 5c) are 0.18 eV and 0.25 eV higher in energy, respectively.

The ground state of Y_3O_4 is predicted to be ^{2}A$_1$ with C_{3v} symmetry (Figure 5d) which is in agreement with the previous report[59]. It is similar to the ground state of $Y_3O_4^-$ cluster in term of atomic connectivity, except all the corresponding bond distances become a little shorter. The nearest low-lying isomer (Figure S5e) with a

terminal and two bridging O atoms is located 0.52 eV higher above the ground state.

3.3 Stoichiometric clusters: $Y_3O_5^{-/0}$

The ground state for $Y_3O_5^-$ is C_s (^{1}A') (Figure 6a), in which three Y atoms transfer a total of ten electrons to oxygen atoms. In the ground state of $Y_3O_5^-$ anionic cluster, the Y–O_t bond distance is 1.926 Å which can be assigned as a typical Y=O double bond[57]. The length of the Y–O_c bond connecting the top Y atom increases to 2.486 Å compared with 2.175 Å in the ground state of the $Y_3O_4^-$ (Figure 5d). A higher symmetry C_{2v} ($^1A_1$) structure is about 0.57 eV above the ground state as shown in Figure S6a.

The ground state of Y_3O_5 is predicted to be ^{2}A" with C_s symmetry (Figure 6b). The Y–O_t bond length is 2.155 Å and about 0.229 Å lengthened compared to that of the anion (Figure 6a). Nevertheless the length of Y–O_c bond connecting the top Y atom becomes a slightly shorter (~ 0.177 Å). Other isomers shown in Figure 6c and 6d are 0.11 eV and 0.21 eV higher, respectively. The results of single-point CCSD(T) calculations with the BP86 geometries within 0.20 eV indicate that the isomer (C_s, ^{2}A") (Figure 6b) is the ground state and the isomer in Figure 6c is 0.19 eV above the ground state.

3.4 Oxygen-rich clusters: $Y_3O_6^{-/0}$

We started the structural searches for the oxygen-rich clusters $Y_3O_6^{-/0}$ by adding one oxygen atom (terminal, capped or bridging oxygen atom) from the structures of $Y_3O_5^{-/0}$ clusters. The ground state of $Y_3O_6^-$ is the C_s (^{1}A') (Figure 7a) structure, which can be viewed as replacing the terminal oxygen in the ground state of $Y_3O_5^-$ (C_s, ^{1}A') (Figure 6a) by an O_2 unit. The calculated O–O bond length of the O_2 unit in the ground state of $Y_3O_6^-$ (Figure 7a) is 1.492 Å, which is close to that of the free peroxide anion O_2^{2-} (1.540 Å calculated at the same level). The triplet state isomers (Figure 7b and Figure 7e) with an O_2 unit are 0.06 eV and 0.27 eV higher in energy, respectively. The third low-lying isomer C_s (^{3}A") (Figure 7c) with two terminal

oxygen atoms is 0.19 eV higher in energy. Single-point CCSD(T) calculations are performed for the low-lying isomers, revealing that isomer (C_s ^{1}A') (Figure 7a) is the global minimum, about 0.60 eV lower than isomer (C_s, ^{3}A") (Figure 7b) in energy.

The neutral ground state C_s (^{2}A") (Figure 7g) shows similar structural characteristics relative to its anion, except that the distance of O_2 unit is shortened. The bond length is 1.353 Å for O_2 unit which is assigned as a superoxide ($O_2^{-\bullet}$) unit (1.361 Å calculated at the same level). Alternative optimized neutral structures are at least 0.72 eV above the ground state (Figure S7, Supporting Information).

4. Discussion

4.1 Interpretation of the Simulated Photoelectron Spectra and Molecular Orbital Analyses

We calculated the vertical detachment energies (VDEs) of $Y_3O_x^-$ (x = 0–6) on the basis of the identified anionic ground-state structures using the generalized Koopmans' theorem. The calculated VDEs and the simulated PES spectra for the global minima are collected in Table 1 and Figure 8, respectively. Others for selected low-lying isomers are listed in Figure S8. All the simulations were done by fitting the distribution of calculated VDEs with unit-area Gaussian functions of 0.10 eV width. In the single-particle picture, photodetachment involves removal of electrons from occupied molecular orbitals (MOs) of an anion. The final states are the ground and excited states of the corresponding neutral. Within the one-electron formalism, each occupied MO for a closed-shell anion will generate a single PES band with the associated vibrational structures governed by the Franck-Condon principle. However, $Y_3O_3^-$ is open-shell with two single unpaired electrons in their lowest-energy structures. In these cases, detachment from a fully occupied MO would result in two detachment channels due to the removal of either the spin-down (α) or the spin-up (β) electrons, giving rise to doublet (D) and quartet (Q) final states, respectively, as given in Table 1. In the following, we will attempt to qualitatively account for the simulated

PES features using molecular orbital analyses. Considering the complicated nature of the electronic structures of these systems, many of the assignments should be considered tentatively.

4.1.1 Metal cluster: Y_3^-

The global minimum of Y_3^- is a D_{3h} ($^1A_1'$) (Figure 1a) structure in our calculation. Its valence electronic configuration is … $(3a_1')^2(4e')^4(2a_2'')^2(4a_1')^2$ as Figure 9a showing. The band X in the simulated PES can be assigned to electrons detachment transition from the MO $4a_1'$ and $2a_2''$, and the VDEs are 1.29 eV for $4a_1'$, 1.32 eV for $2a_2''$, respectively. While removing an electron from Y_3^-, the ground state of Y_3 would still maintain the equilateral triangular structure. As shown in Figure 9a, $4a_1'$ is a bonding orbital, thus the detachment from $4a_1'$ makes the Y–Y bond length increase from 3.094Å to 3.160 Å (Figure 1a and 1e). The band A is calculated to be about 1.68 eV, which can be assigned to electron detachment transition from the degenerate orbital HOMO-2 (4e'). The HOMO-3 ($3a_1'$) is a bonding MO composed mainly of s orbitals from the three Y atoms. Its corresponding VDE is 3.09 eV which is relatively high.

4.1.2 Oxygen-deficient clusters: $Y_3O_x^-$ (x = 1–4)

As mentioned earlier, our DFT calculations and further CCSD(T) optimizations indicate that isomer C_{3v} ($^1A_1$) (Figure 2a) is the lowest-energy structure of Y_3O^-. It can be regarded as adding a capped oxygen atom based on the ground state of Y_3^- (Figure 1a). Its valence electronic configuration is … $(6a_1)^2(6e)^4(7a_1)^2$ as shown in the Figure 9b. The calculated VDE (1.20 eV) for the first detachment channel from $7a_1$ MO is in excellent agreement with the experimental measurement of 1.25 eV[14]. The corresponding bonding MO $7a_1$ primarily consists of d orbitals from the three Y atoms. Two sharper features (X, A) are displayed at lower binding energies which coincides with the experimental spectrum[14] and the second detachment channel is from 6e MOs (Figure 9b) with the calculated VDE of 1.56 eV. For the low-lying isomer (Figure 2b) which is the powerful competitor for the ground state of Y_3O^- in the CCSD(T) optimization level, the simulated photoelectron spectra (Figure S8a)

displays only one detachment channel (within 2.00 eV) which is distinct with the experimental spectrum[14].

For $Y_3O_2^-$, the ground state of $Y_3O_2^-$ is a closed-shell (^{1}A') C_s (Figure 3a) configuration with a capped and a bridging O atoms. The calculated first VDE for the lowest energy structure C_s (^{1}A') (Figure 3a) is 1.37 eV at the BP86 level, which is closed to that of 1.60 eV measured by experiment[14] and the second VDE (1.38 eV) is only 0.01 eV higher than the first VDE. Its valence electronic configuration shown in the Figure 9c is … $(16a')^2(8a'')^2(17a')^2$. Therefore, photodetachment from HOMO (17a') and HOMO-1 (8a'') orbitals yield the first PES band X (Figure 7c). It is only about 0.17 eV higher above that (1.20 eV) of Y_3O^- because of the nonbonding (17a') orbital.

The ground state of $Y_3O_3^-$ is an open shell C_s (^{3}A'') structure which can be viewed as adding a bridging O atom on the basis of $Y_3O_2^-$. Its valence electronic configuration is … $(17a')^2(12a'')^1(18a')^1$. The first detachment channel for the $Y_3O_3^-$ (C_s, ^{3}A'') ground state is derived from the orbital 18a' (α) with the calculated VDE of 1.43 eV which is in good consistency with the previous experimental value (1.52 eV)[14]. Figure 9d presents the molecular orbitals of $Y_3O_3^-$. The HOMO 18a' consists of a Y 5s character which makes the first VDE increase slightly contrasting to Y_3O^- and $Y_3O_2^-$. The second detachment channel is from 12a'' (α) with the calculated VDE of 1.69 eV and the band B is yielded by detaching the electron from the full occupied 17a' (α, β) orbital with different VDEs of 2.37 eV and 2.19 eV, respectively.

In the $Y_3O_4^-$ anion, the results of single-point CCSD(T) calculations manifest that the isomer with a capped and three bridging O atoms is the global minimum. Its valence electron configuration is … $(17a_1)^2(10e)^4(18a_1)^2$. The calculated VDE for the band X is 1.05 eV. In Figure 9e, the HOMO mainly consists of Y 5s character, contributed equally by each of three Y atoms. Similar to the study by Wu[58], each Y atom possesses three valence electrons and three Y atoms will lose a total of eight electrons forming the $Y_3O_4^-$ cluster. The orbital analysis indicates that the rest of 5s electrons are distributed by the three yttrium atoms.

4.1.3 Stoichiometric cluster: $Y_3O_5^-$

The ground state for $Y_3O_5^-$ is a closed-shell structure with C_s (^{1}A') symmetry (Figure 6a) and it appears a terminal O atom based on $Y_3O_4^-$. In the stoichiometric $Y_3O_5^-$ cluster, all Y atoms possess the maximum +3 oxidation state, each of which is chemically saturated, and O atoms possess –2 oxidation state. The valence electron configuration of $Y_3O_5^-$ is … $(23a')^2(13a'')^2(24a')^2$. The large VDE value (2.47 eV) observed in our PES spectrum is consistent with the fact that $Y_3O_5^-$ should be a relatively stable molecule. In $Y_3O_5^-$, all the 4d or 5s electrons are transferred from Y to O and the increase for the first VDE of $Y_3O_5^-$ is mainly on account of the terminal O 2p features.

4.1.4 Oxygen-rich clusters: $Y_3O_6^-$

The ground state of $Y_3O_6^-$ is C_s (^{1}A') which can be viewed as replacing a terminal O atom in $Y_3O_5^-$ by an O_2 unit. The O_2 unit can be viewed as peroxide anion O_2^{2-} with a 1.492 Å O–O bond. We can estimate primarily that the addition of two electrons into the π^* orbital lengthen the O–O bond. The valence electron configuration of anionic $Y_3O_6^-$ is … $(26a')^2(27a')^2(14a'')^2$. The calculated VDE for the band X is 1.97 eV corresponding to detachment of p electrons on HOMO which is a π^* orbital of O_2 unit. Thus, detachment from the 14a'' orbital results in the O_t–O_t distance significant decrease in the neutral cluster (Figure 7g).

4.2 Structural Evolution and Sequential Oxidation of $Y_3O_x^-$ (x = 1–6)

The current study shows that the ground states of $Y_3O_x^-$ (x = 1–6) clusters are all the structures with a capped oxygen atom. Starting from Y_3^- triangle structure, the ground state of Y_3O^- is found to be a pyramid in which the capped oxygen atom is above the plane of tri-yttrium equilateral triangle. The next three oxygen atoms successively take up the bridging sites until $Y_3O_4^-$ which is based on a six-membered Y_3O_3 ring adding a capped oxygen atom. On the basis of the ground state of $Y_3O_4^-$, the next added oxygen atom is shown to occupy the terminal site forming $Y_3O_5^-$ and the ground state of $Y_3O_6^-$ can be viewed as replacing a terminal O atom in $Y_3O_5^-$ by

an O_2 unit. In Figure 10, the trend of electron affinities (EAs) is consistent with that of first VDEs until Y_3O_4, which indicates the corresponding anionic and neutral clusters $Y_3O_x^{-/0}$ (x = 1–4) possess the similar geometric configurations.

Figure 10 displays the trend of the first VDEs for $Y_3O_x^-$ (x = 1–6). The first VDEs of the $Y_3O_x^-$ (x = 1−4) oxide clusters are all around 1.0 eV, and 1.20 eV for Y_3O^-, 1.37 eV for $Y_3O_2^-$, 1.43 eV for $Y_3O_3^-$, 1.05 eV for $Y_3O_4^-$. As for $Y_3O_5^-$, the first VDE rises to 2.47 eV, whereas the first VDE for $Y_3O_6^-$ decreases to 1.97 eV. Y has an electron configuration of $4d^15s^2$, and the bare tri-yttrium anion Y_3^- has 10 valence electrons. The Y-derived valence electrons sequentially transfer to the added oxygen atoms with the x increasing. The values of first VDEs for $Y_3O_x^-$ (x = 1–4) slightly change as a function of O content. The higher binding energy for $Y_3O_5^-$ can be illuminated by the nature of the HOMO (24a') (Figure 9f), which is primarily the terminal oxygen atom 2p-based orbital. The first VDE for $Y_3O_6^-$ is descending compared with that for $Y_3O_5^-$ because of the electrons derived from π^* molecular orbital. The trend of VDEs in $Y_3O_x^-$ (x = 1–6) is consistent with previous studies of metal oxide clusters[23,60–64], suggesting a sequential oxidation of the metal oxides clusters.

4.3. All-metal aromaticity of Y_3^-

4.3.1 The molecular orbital analysis

The global minimum of Y_3^- is a D_{3h} ($^1A_1'$) structure (Figure 1a). In the early time, Feixas [32] reported that Y_3^- has σ- and π-aromaticity with the nucleus-independent chemical shifts (NICS) values. To further understand the electronic structure and chemical bonding in the Y_3^- cluster, a detailed molecular orbital (MO) analysis is carried out as shown in Figure 9a. The full-filled $3a_1'$ and 4e' are a set of completely bonding and partially bonding/antibonding and should not contribute to the net aromaticity significantly in the Y_3^- cluster. The fully occupied $2a_2''$ MO is made up of the 4d orbitals of Y atoms, and is of π-aromatic character. The $4a_1'$ MO is completely

delocalized σ bonding composed primarily of the 4d orbital of each Y atom, which is responsible for d-orbital σ-aromatic character according to the (4n+2) Hückel rule for σ aromaticity[65]. Thus, the Y_3^- D_{3h} ($^1A_1'$) can be considered as a case of d-orbital σ- and π-aromaticity, which is very similar to the Sc_3^- cluster[28].

4.3.2 AdNDP analysis

In order to further verify the aromaticity of Y_3^-, AdNDP analysis is used to figure out the ways of its chemical bonding. The AdNDP program can obtain the electronic structure in terms of n-center two-electron (nc-2e) bonds. It reveals both localized Lewis bonding and delocalized bonding elements (nc-2e objects, n⩾3), which are associated with the concepts of aromaticity and antiaromaticity[54]. There are 10 valence electrons in Y_3^-, which form 5 valence electronic pairs. According to the AdNDP analysis (Figure 11), these pairs are revealed as follows: three 2c-2e Y-Y σ-bonds between two yttrium atoms with ON = 1.99|e|, a completely delocalized 3c-2e d-orbital π-bond with ON = 2.00|e| and a 3c-2e d-orbital σ-bond with ON = 2.00|e|, in which ON represents the occupied number. Therefore the Y_3^- cluster has a double (σ- and π-) aromaticity via the AdNDP analysis.

4.4 $Y_3O_4^{-/0}$ as Reduced Molecular Models for Dioxygen Activation: $Y_3O_4^{-/0} + O_2 \rightarrow Y_3O_6^{-/0}$.

As mentioned earlier, the ground states of Y_3O_6 (Figure 7g) and $Y_3O_6^-$ (Figure 7a) clusters can be viewed as adding a superoxide $O_2^{-\bullet}$ and peroxide O_2^{2-} units on Y_3O_4 and $Y_3O_4^-$ clusters, respectively. The observation of O_2 units in Y_3O_6 and $Y_3O_6^-$ provides us with an excellent opportunity to study the activation of O_2 by the Y_3O_4 and $Y_3O_4^-$ clusters. The energies of the O_2 addition reactions are evaluated at the BP86 level:

$$Y_3O_4\,(C_{3v},\,^2A_1) + O_2 \rightarrow Y_3O_6\,(C_s,\,^2A'') \quad -2.97\ \text{eV} \qquad (1)$$

$$Y_3O_4^-\,(C_{3v},\,^1A_1) + O_2 \rightarrow Y_3O_6^-\,(C_s,\,^1A') \quad -3.25\ \text{eV} \qquad (2)$$

The equations (1) and (2) can be viewed as the reactions of O_2 with the ground

states of Y_3O_4 and $Y_3O_4^-$, respectively. Our calculation yielded the O_2 chemisorption energy of –2.97 eV in Y_3O_4 and –3.25 eV in $Y_3O_4^-$, respectively. Similar to our previous studies of metal oxide clusters[22,66–68], molecular orbitals in the O-rich systems are analyzed to gain further insight into the nature of the chemical bonding. The orbitals of Y_3O_6 are illustrated in Figure 12. The singly occupied MO is one of the two π* orbitals of the bound O_2 unit, and the HOMO are doubly occupied π* orbital of O_2 that is singly occupied in free O_2. The O–O distance (1.353 Å) in Y_3O_6 (Figure 6g) is longer than that in free O_2 and is close to that in superoxide $O_2^{-\bullet}$ unit. It shows that the rest of 5s electron of Y_3O_4 may be readily transferred to the π* orbitals of an approaching O_2 molecule, making Y_3O_4 a reductive agent for O_2 activation. Analogously, the O–O distance (1.492 Å) in $Y_3O_6^-$ (Figure 7a) is close to that in peroxide O_2^{2-} unit and the extra two 5s electrons of $Y_3O_4^-$ may be transferred to the π* orbitals of an approaching O_2 molecule. Therefore, the Y_3O_6 and $Y_3O_6^-$ clusters can be considered as the oxidation products for the activation of O_2 through electron transfer between the reduced metal site and dioxygen at the metal oxide surface.

5. Conclusion

We report a systematic photoelectron spectroscopy and density functional study of a series of tri-nuclear yttrium oxide clusters: $Y_3O_x^-$ and Y_3O_x (x = 0–6). Extensively DFT calculations are performed at the BP86 level to locate the ground states for the $Y_3O_x^{-/0}$ (x = 0–6) cluster. The ground states for Y_3^- and Y_3 are D_{3h} (^{1}A') and D_{3h} (^{2}A$_1$') structures, respectively. The tri-yttrium oxide clusters $Y_3O_x^{-/0}$ (x = 1–6) all have a capped oxygen atom. Starting from Y_3O^-, successively adding bridging oxygen atoms yield the ground states of $Y_3O_2^-$, $Y_3O_3^-$ and $Y_3O_4^-$. Nevertheless, the next added oxygen atom is found to be a terminal one in $Y_3O_5^-$ cluster and the oxygen-rich cluster $Y_3O_6^-$ is found to own an O_2 unit. The neutral species have similar structures with their corresponding anionic clusters. As for the oxygen-rich clusters $Y_3O_6^-$ and Y_3O_6, O_2^{2-} and $O_2^{-\bullet}$ units are found which can be viewed as $Y_3O_4^-$ and Y_3O_4 are oxidized by the O_2, respectively. Molecular orbital analyses are carried out

to elucidate the chemical bonding of these clusters and provide insights into the sequential oxidation from Y_3O^- to $Y_3O_6^-$. The molecular orbital analysis presents that Y_3^- (D_{3h}, $^1A_1'$) possesses σ- and π-aromaticity. The AdNDP analysis reveals that one 3c-2e σ-bond and one 3c-2e π-bond completely delocalized over the three yttrium atoms, which further proves the characteristic of aromaticity in the Y_3^- cluster.

Acknowledgments

We gratefully acknowledge supports from the National Natural Science Foundation of China (21071031, 21301030, 21371034 and 21373048), and the Natural Science Foundation of Fujian Province for Distinguished Young Investigator Grant (2013J06004).

Reference

1 D. Kima, S. Jeonga, J. Moona and S. H. Cho, *J. Colloid Interf. Sci.*, 2006, **297**, 589.

2 P. V. A. Padmanabhan, S. Ramanathan, K. P. Sreekumar, R. U. Satpute, T. R. G. Kutty, M. R. Gonal and L. M. Gantayet, *Mater. Chem. Phys.*, 2007, **106**, 416.

3 A. M. Pires, O. A. Serra and M. R. Davolos, *J. Lumin.*, 2005, **113**, 174.

4 W. J. Song, J. S. Li, T. B. Zhang, H. C. Kou and X. Y. Xue, *J. Power Sources*, 2014, **245**, 808.

5 Y. Chen, J. Bunch, C. Jin, C. H. Yang and F. L. Chen, *J. Power Sources*, 2012, **204**, 40.

6 V. Singh, V. K. Rai, B. Voss, M. Haase, R. P. S. Chakradhar, D. T. Naidu and S. H. Kim, 2013, **109**, 206.

7 A. M. Pires, O. A. Serra and M. R. Davolos, *J. Alloy. Compd.*, 2004, **374**, 181.

8 N. Al-Yassir and R. L. V. Mao, *Can. J. Chem.*, 2008, **86**, 146.

9 N. Al-Yassir and R. L. V. Mao. *Appl. Catal. A-Gen.*, 2007, **317**, 275.

10 J. B. Ma, Z. C. Wang, M. Schlangen, S. G. He and H. Schwarz, *Angew. Chem. Int. Ed.*, 2013, **52**, 1226.

11 V. V. Lavrov, V. Blagojevic, G. K. Koyanagi, G. Orlova and D. K. Bohme. *J. Phys. Chem. A*, 2004, **108**, 5610.

12 M. Knickelbein, *Chem. Phys.*, 1995, **102**, 1.

13 H. B. Wu and L. S. Wang, *J. Phys. Chem. A*, 1998, **102**, 9129.

14 A. Pramann, Y. Nakamura and A. Nakajima, *J. Phys. Chem. A*, 2001, **105**, 7534.

15 G. Gu, B. Dai, X. Ding and J. Yang, *Eur. Phys. J. D*, 2004, **29**, 27.

16 B. Dai, K. Deng and J. Yang. *Chem. Phys. Lett.*, **2002**, 364, 188.

17 Z. Yang, S. J. Xiong, *J. Chem. Phys*., 2008, **129**, 124308.

18 A. B. Rahane, P. A. Murkute, M. D. Deshpande and V. Kumar, *J. Phys. Chem. A*, 2013, **117**, 5542.

19 H. J. Zhai, X. Huang, T. Waters, X. B. Wang, R. A. J. O'Hair, A. G. Wedd and L. S. Wang, *J. Phys. Chem. A*, 2005, **109**, 10512.

20 H. J. Zhai, X. Huang, L. F. Cui, X. Li, J. Li and L. S. Wang, *J. Phys. Chem. A*, 2005, **109**, 6019.

21 H. J. Zhai, B. Wang, X. Huang and L. S. Wang, *J. Phys. Chem. A*, 2009, **113**, 9804.

22 B. Wang, W. J. Chen, B. C. Zhao, Y. F. Zhang and X. Huang, *J. Phys. Chem. A*, 2010, **114**, 1964.

23 W. J. Chen, H. J. Zhai, Y. F. Zhang, X. Huang and L. S. Wang, *J. Phys. Chem. A*, 2010, **114**, 5958.

24 Q. Zhou, W. C. Gong, L. Xie, C. G. Zheng, W. Zhang, B. Wang, Y. F. Zhang and X. Huang, *Spectrochim. Acta. A*, 2014, **117**, 651.

25 B. Wang, H. J. Zhai, X. Huang and L. S. Wang, *J. Phys. Chem. A*, 2008, **112**, 10962.

26 P. W. Fowler, R. W. A. Havenith and E. Steiner, *Chem. Phys. Lett.*, 2002, **359**, 530.

27 B. B. Averkiev and A. I. Boldyrev, *J. Phys. Chem. A*, 2007, **111**, 12864.

28 T. R. Galeev and A. I. Boldyrev, *Annu. Rep. Prog. Chem., Sect. C*, 2011, **107**, 124.

29 A. E. Kuznetsov, J. D. Corbett, L. S. Wang and A. I. Boldyrev, *Angew. Chem. Int. Ed*. 2001, **40**, 3369.

30 Z. Badri, S. Pathak, H. Fliegl, P. Rashidi-Ranjbar, R. Bast, R. Marek, C. Foroutan-Nejad and K. Ruud, *J. Chem. Theory Comput.*, 2013, **9**, 4789.

31 X. X. Chi and Y. Liu, *Int. J. Quantum Chem.*, 2007, **107**, 1886.

32 F. Feixas, E. Matito, M. Duran, J. Poater and M. Sol, *Theor. Chem. Acc.*, 2011, **128**, 419.

33 A. E. Kuznetsov, K. A. Birch, A. I. Boldyrev, X. Li, H. J. Zhai and L. S. Wang, *Science*, 2003, **300**, 622.

34 H. J. Zhai, W. J. Chen, X. Huang and L. S. Wang, *RSC Adv.*, 2012, **2**, 2707.

35 X. Huang, H. J. Zhai, B. Kiran and L. S. Wang, *Angew. Chem. Int. Ed.*, 2005, **44**, 7251.

36 A. D. Becke, *Phys. Rev. A*, 1988, **38**, 3098.

37 J. P. Perdew, *Phys. Rev. B*, 1986, **33**, 8822.

38 W. Küchle, M. Dolg, H. Stoll and H. Preuss, Pseudopotentials of the Stuttgart/Dresden group 1998, revision August 11, 1998: http://www.theochem.uni-stuttgart.de/pseudopotentiale.

39 D. Andrae, U. Haeussermann, M. Dolg, H. Stoll and H. Preuss, *Theor. Chim. Acta.*, 1990,**77**, 123.

40 J. M. L. Martin and A. Sundermann, *J. Chem. Phys.*, 2001, **114**, 3408.

41 R. A. Kendall, T. H. Dunning and *R*. J. Harrison, *J. Chem. Phys.*, 1992, **96**, 6796.

42 T. H. Dunning, *J. Chem. Phys.*, 1989, **90**, 1007.

43 D. J. Tozer and N. C. Handy, *J. Chem. Phys*., 1998, **109**, 10180.

44 G. D. Purvis and R. J. Bartlett, *J. Chem. Phys*., 1982, **76**, 1910.

45 G. E. Scuseria, C. L. Janssen and H. F. Schaefer III, *J. Chem. Phys.*, 1988, **89**, 7382.

46 K. Raghavachari and G. W. Trucks, *Chem. Phys. Lett.*, 1989, **157**, 479.

47 J. D. Watts, J. Gauss and R. J. Bartlett, *J. Chem. Phys*., 1993, **98**, 8718.

48 R. J. Bartlett and M. Musiał, *Rev. Mod. Phys.*, 2007, **79**, 291.

49 M. J. Frisch, G. W. Trucks, H. B. Schlegel, G. E. Scuseria, M. A. Robb, J. R. Cheeseman, G. Scalmani, V. Barone, B. Mennucci, G. A. Petersson, H. Nakatsuji, M. Caricato, X. Li, H. P. Hratchian, A. F. Izmaylow, J. L. Sonnenberg, M. Hada, M. Ehara, K .Toyota, R. Fukuda, J. Hasegawa, M. Ishida, T. Nakajima, Y. Honda, O. Kitao, H. Nakai, T. Vreven, J. A. Montgomery, Jr., J. E. Peralta, F. Ogliaro, M. Bearpark, J. J. Heyd, E. Brothers, K. N. Kudin, V. N. Staroverov, R. Kobayashi, J. Normand, K. Raghavachari, A. Rendell, J. C. Burant, S. S. Iyengar, J. Tomasi, M. Cossi, N. Rega, J. M. Millam, M. Klene, J. E. Knox, J. B. Cross, V. Bakken, C. Adamo, J. Jaramillo, R. Gomperts, R. E. Stratmann, O. Yazyev, A. J. Austin, R. Cammi, C. Pomelli, J. W. Ochterski, R. L. Martin, K. Morokuma, V. G. Zakrzewski, G. A. Voth, P. Salvador, J. J. Dannenberg, S. Dannenberg, S. Dapprich, A. D. Daniels, O. Farkas, J. B. Foresman, J. V. Ortiz, J. Cioslowski, and D. J. Fox, Gaussian 09, Revision A.1, Gaussian, Inc., Wallingford CT, 2009.

50 H. J. Werner, P. J. Knowles, F. R. Manby, M. Schütz, P. Celani, G. Knizia, T. Korona, R. Lindh, A. Mitrushenkov, G. Rauhut, T. B. Adler, R. D. Amos, A. Bernhardsson, A. Berning, D. L. Cooper, M. J. O. Deegan, A. J. Dobbyn, F. Eckert, E. Goll, C. HamPel, A. Hesselmann, G. Hetzer, T. Hrenar, G. Jansen, C. KöPPl, Y. Liu, A. W. Lloyd, R. A. Mata, A. J. May, S. J. McNicholas, W. Meyer, M. E. Mura, A. Nicklass, D. P. O'Neill, P. Palmieri, K. Pflüger, R. Pitzer, M. Reiher, T. Shiozaki, H. Stoll, A. J. Stone, R. Tarroni, T. Thorsteinsson, M. Wang and A. Wolf, MOLPRO, version 2010.1, a package of ab initio programs; See http://www.molpro.net.

51 W. Humphrey, A. Dalke and K. Schulten, *J. Mol. Graphics*, 1996, **14**, 33.

52 L. Andrews, M. F. Zhou and G. V. Chertihin, *J. Phys. Chem. A*, 1999, **103**, 6525.

53 Y. Gong, C.F. Ding and M.F. Zhou, *J. Phys. Chem. A*, 2009, **113**, 8569.

54 D. Yu. Zubarev and A. I. Boldyrev, *Phys. Chem. Chem. Phys.*, 2008, **10**, 5207.

55 U. Varetto, Molekel5.4, Swiss National Supercomputing Centre, Manno, Switzerland, 2009.

56 D. Dai and K. Balasubramanian, *J. Chem. Phys.*, 1993, **98**, 7098.

57 Y. X. Zhao, X. L. Ding, Y. P. Ma, Z. C. Wang and S. G. He, *Theor. Chem. Acc.*, 2010, **127**, 449.

58 Z. Yang and S. J. Xiong, *J. Phys. B: At. Mol. Opt. Phys.*, 2009, **42**, 245101.

59 L. Wu, C. Zhang, S. A. Krasnokutski and D.S. Yang, *J. Chem. Phys.*, 2012, **137**, 084312.

60 H. Wu, X. Li, X. B. Wang, C. F. Ding and L. S. Wang, *J. Chem. Phys.*, 1998, **109**, 449.

61 L. S. Wang, H. Wu and S. R. Desai, *Phys.Rev.B*, 1995, **53**, 8028.

62 L. S. Wang, H. Wu and S.R. Desai, *Phys. Rev. Lett.*, 1996, **76**, 4853.

63 S. J. Lin, X. H. Zhang, L. Xu, B. Wang, Y. F. Zhang and X. Huang, *J. Phys. Chem. A*, 2013, **117**, 3093.

64 L. F. Wang, L. Xie, H. L. Fang, Y. F. Li, X. B. Zhang, B. Wang, Y. F. Zhang and X. Huang, *Spectrochim. Acta. A*, 2014, **131**, 446.

65 A. P. Sergeeva, B. B. Averkiev and A. I. Boldyrev, *Struct. Bond.*, 2010, **136**, 275.

66 H. J. Zhai, X. H. Zhang, W. J. Chen, X. Huang and L. S. Wang, *J. Am. Chem. Soc.*, 2011, **133**, 3085.

67 X. Huang, H. J. Zhai, T. Waters, J. Li and L. S. Wang, *Angew. Chem. Int. Ed.*, 2006, **45**, 657.

68 S. J. Lin, W. C. Gong, L. F. Wang, W. B. Liu, B. C. Zhao, B. Wang, Y. F. Zhang , X. Huang, *Theor. Chem. Acc.*, 2014, **133**, 1435.

FIGURE CAPTIONS

Figure 1 Optimized global minima and selected low-lying structures (within ~ 0.40 eV) for $Y_3^{-/0}$ clusters at the BP86 level. The bond lengths are in angstroms.

Figure 2 Optimized global minima and selected low-lying structures (within ~ 0.40 eV) for $Y_3O^{-/0}$ clusters at the BP86 level. The bond lengths are in angstroms.

Figure 3 Optimized global minima and selected low-lying structures (within ~ 0.40 eV) for $Y_3O_2^{-/0}$ clusters at the BP86 level. The bond lengths are in angstroms.

Figure 4 Optimized global minima and selected low-lying structures (within ~ 0.40 eV) for $Y_3O_3^{-/0}$ clusters at the BP86 level. The bond lengths are in angstroms.

Figure 5 Optimized global minima and selected low-lying structures (within ~ 0.40 eV) for $Y_3O_4^{-/0}$ clusters at the BP86 level. The bond lengths are in angstroms.

Figure 6 Optimized global minima and selected low-lying structures (within ~ 0.40 eV) for $Y_3O_5^{-/0}$ clusters at the BP86 level. The bond lengths are in angstroms.

Figure 7 Optimized global minima and selected low-lying structures (within ~ 0.40 eV) for $Y_3O_6^{-/0}$ clusters at the BP86 level. The bond lengths are in angstroms.

Figure 8 The simulated photoelectron spectra for the global minima of $Y_3O_x^-$ (x = 0–6). The simulations are done by fitting the distribution of calculated vertical detachment energies with unit-area Gaussian functions of 0.10 eV width.

Figure 9 Pictures of the valence molecular orbitals for the ground states of $Y_3O_x^-$ (x = 0–6) clusters.

Figure 10 The first vertical detachment energies and electron affinities for the ground states $Y_3O_x^-$ (x = 1–6) clusters as a function of O content.

Figure 11 Chemical-bonding elements revealed by the AdNDP analysis of the Y_3^- cluster. The ONs are reported at the BP86/lanl2dz level of theory.

Figure 12 Molecular orbital pictures of two highest-energy occupied orbitals of Y_3O_6.

Table 1 Theoretical vertical detachment energies (VDEs) of global minima $Y_3O_x^-$ (x = 0–6) clusters (all energies are in eV).

Figure 1

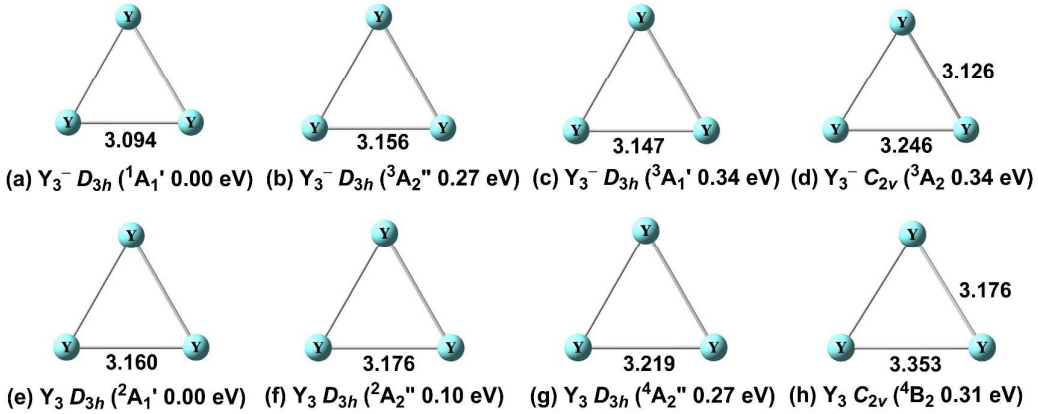

(a) Y_3^- D_{3h} ($^1A_1$' 0.00 eV) (b) Y_3^- D_{3h} ($^3A_2$" 0.27 eV) (c) Y_3^- D_{3h} ($^3A_1$' 0.34 eV) (d) Y_3^- C_{2v} ($^3A_2$ 0.34 eV)

(e) Y_3 D_{3h} ($^2A_1$' 0.00 eV) (f) Y_3 D_{3h} ($^2A_2$" 0.10 eV) (g) Y_3 D_{3h} ($^4A_2$" 0.27 eV) (h) Y_3 C_{2v} ($^4B_2$ 0.31 eV)

Figure 2

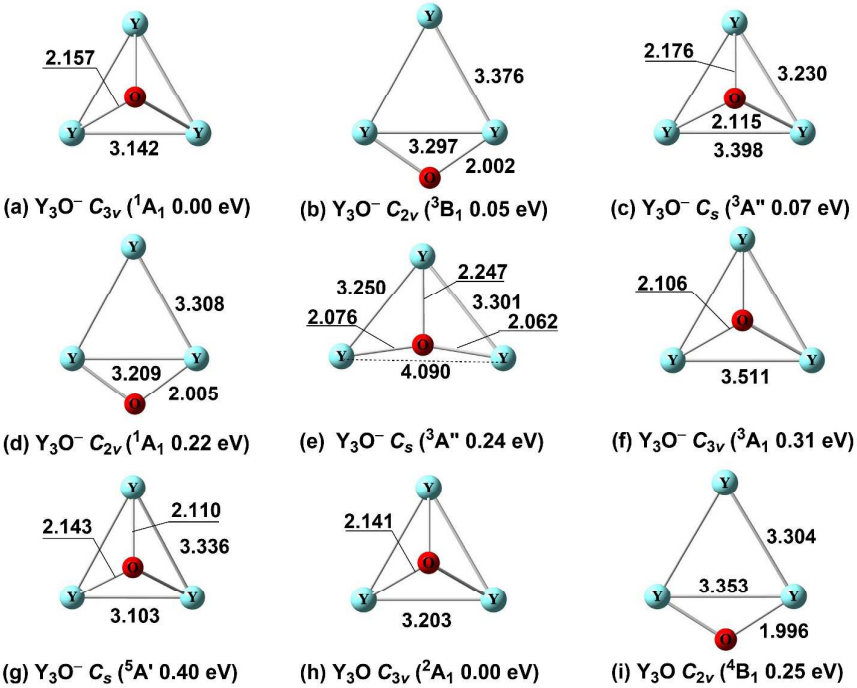

(a) Y_3O^- C_{3v} ($^1A_1$ 0.00 eV) (b) Y_3O^- C_{2v} ($^3B_1$ 0.05 eV) (c) Y_3O^- C_s (^3A" 0.07 eV)

(d) Y_3O^- C_{2v} ($^1A_1$ 0.22 eV) (e) Y_3O^- C_s (^3A" 0.24 eV) (f) Y_3O^- C_{3v} ($^3A_1$ 0.31 eV)

(g) Y_3O^- C_s (^5A' 0.40 eV) (h) Y_3O C_{3v} ($^2A_1$ 0.00 eV) (i) Y_3O C_{2v} ($^4B_1$ 0.25 eV)

Figure 3

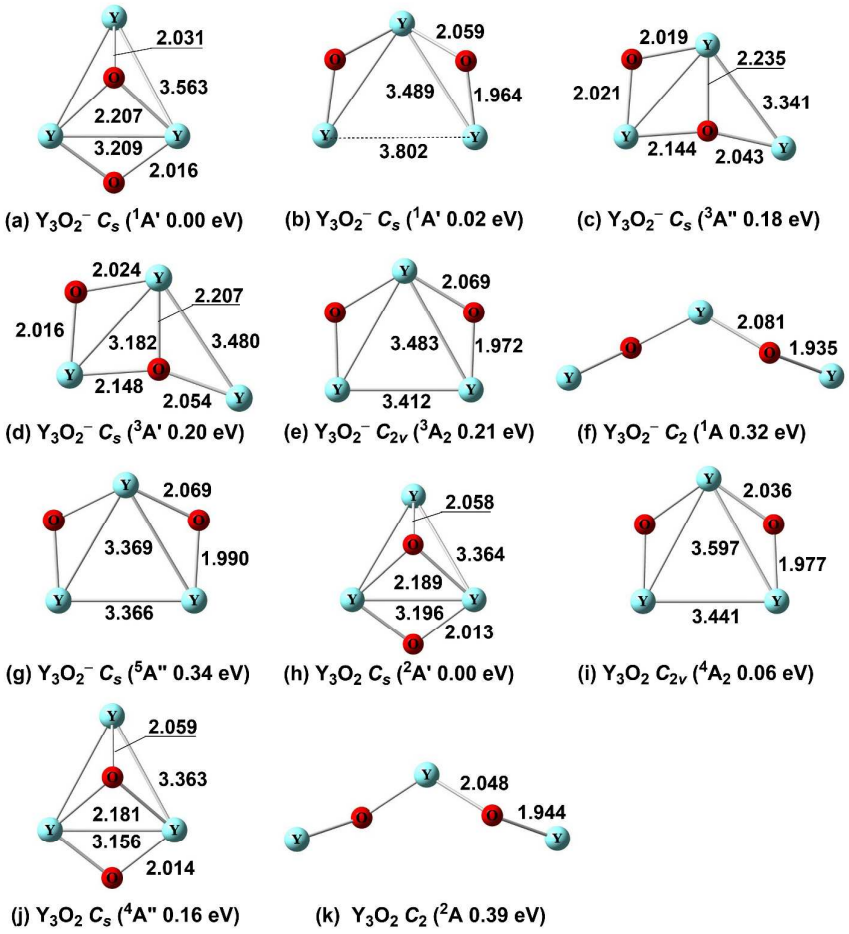

Figure4

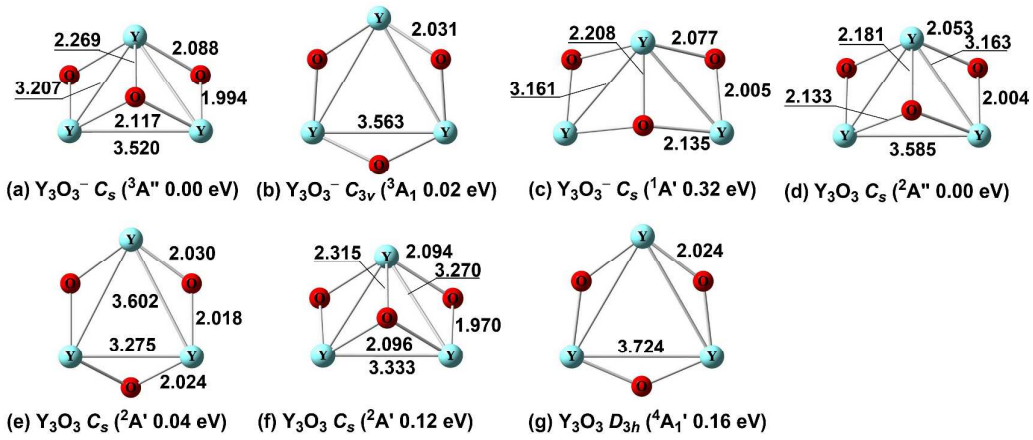

Figure 5

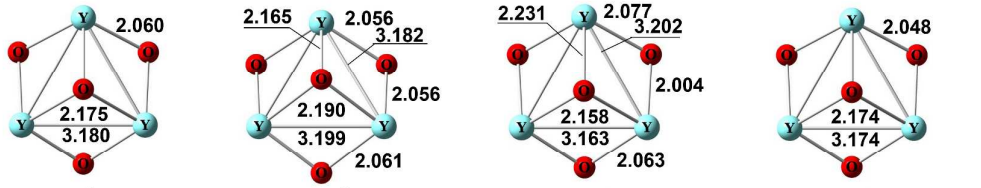

(a) $Y_3O_4^-$ C_{3v} ($^1A_1$ 0.00 eV) (b) $Y_3O_4^-$ C_s ($^3A''$ 0.00 eV) (c) $Y_3O_4^-$ C_s ($^3A'$ 0.06 eV) (d) Y_3O_4 C_{3v} ($^2A_1$ 0.00 eV)

Figure 6

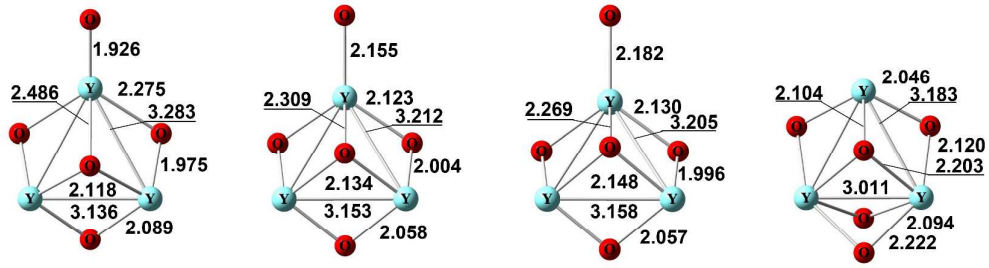

(a) $Y_3O_5^-$ C_s ($^1A'$ 0.00 eV) (b) Y_3O_5 C_s ($^2A''$ 0.00 eV) (c) Y_3O_5 C_s ($^2A'$ 0.11 eV) (d) Y_3O_5 C_s ($^2A'$ 0.21 eV)

Figure 7

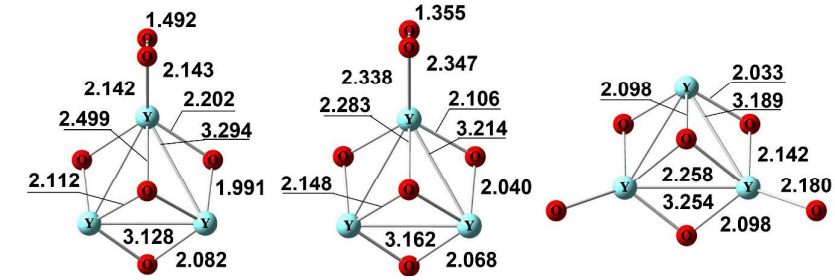

(a) $Y_3O_6^-$ C_s ($^1A'$ 0.00 eV) (b) $Y_3O_6^-$ C_s ($^3A''$ 0.06 eV) (c) $Y_3O_6^-$ C_s ($^3A''$ 0.19 eV)

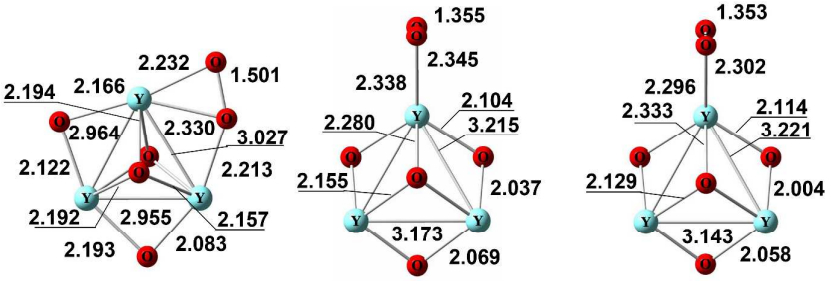

(d) $Y_3O_6^-$ C_s ($^1A'$ 0.23 eV) (e) $Y_3O_6^-$ C_s ($^3A'$ 0.27 eV) (g) Y_3O_6 C_s ($^2A''$ 0.00 eV)

Figure 8

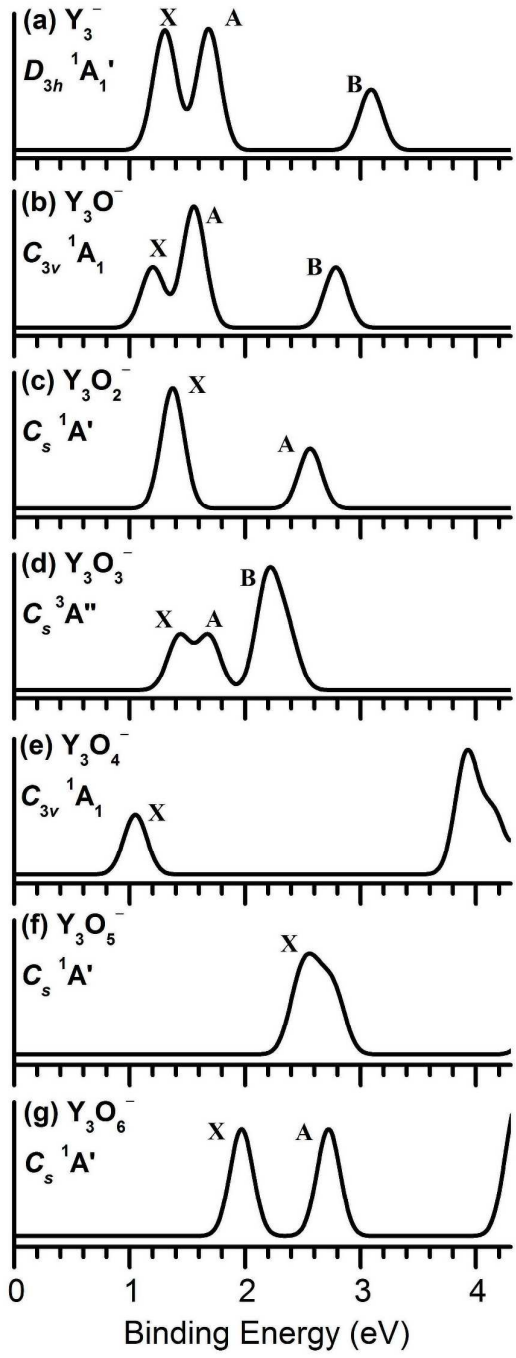

Figure 9

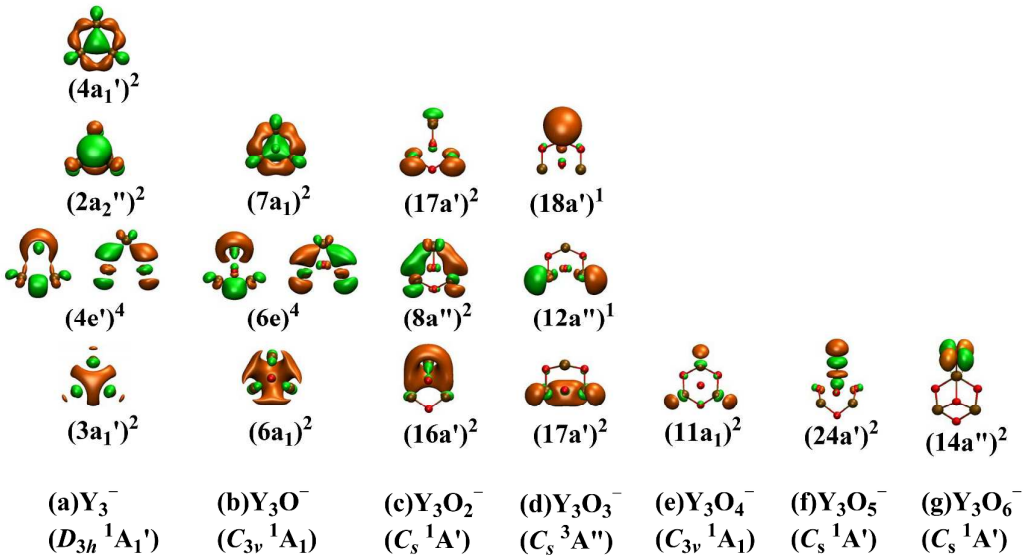

Figure 10

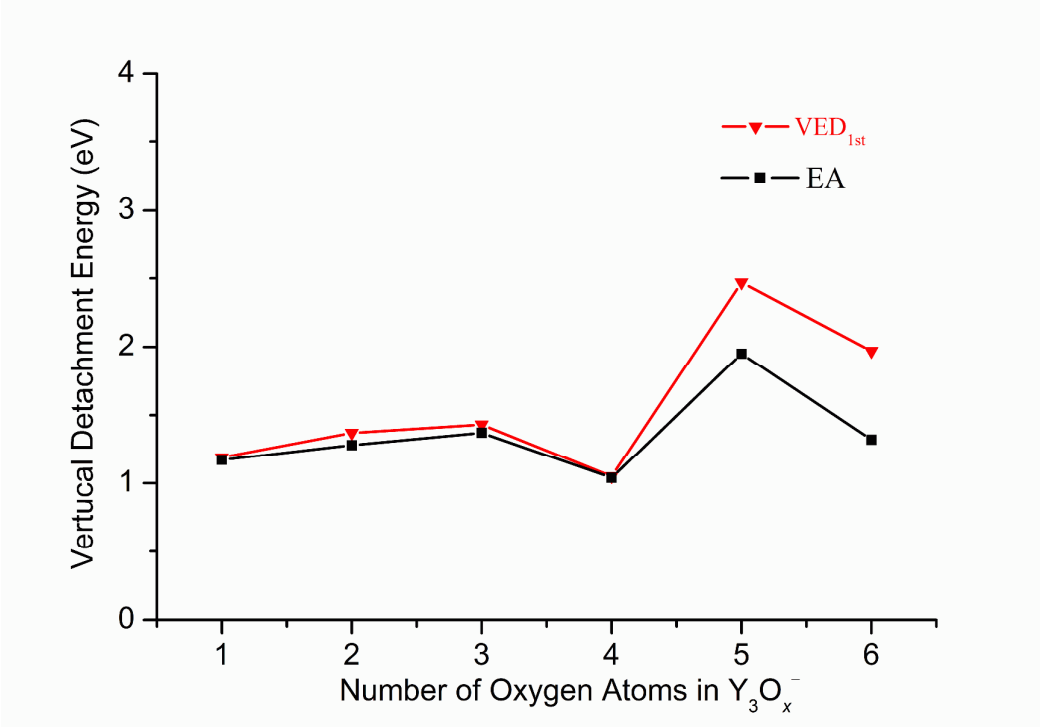

Figure 11

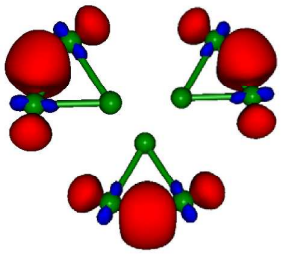

3*(2c-2e) Y–Y σ bonds
ON = 1.99|e|

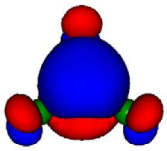

3c-2e Y–Y π bond
ON = 2.00|e|

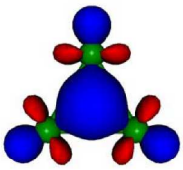

3c-2e Y–Y σ bond
ON = 1.99|e|

Figure 12

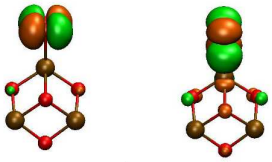

SOMO $(14a'')^1$ HOMO $(27a')^2$

Y_3O_6 (C_s $^2A''$)

Table 1

	Theory[a]		
	Feature[b]	MO	VDE
Y_3^-	X	$4a_1'$	1.29
(D_{3h} $^1A'$)		$2a_2''$	1.32
	A	4e	1.68
			1.68
	B	$3a_1'$	3.09
Y_3O^-	X	$7a_1$	1.20
(C_{3v} $^1A_1$)	A	6e	1.56
			1.56
	B	$6a_1$	2.79
$Y_3O_2^-$	X	17a'	1.37
(C_s $^1A'$)		8a''	1.38
	A	16a'	2.56
$Y_3O_3^-$	X	18a' (α)	1.43 (D)
(C_s $^3A''$)	A	12a'' (α)	1.69 (D)
	B	17 a' (α);[17 a' (β)]	2.37(D); [2.19 (Q)]
$Y_3O_4^-$	X	$11a_1$	1.05
(C_{3v} $^1A_1$)	A	10e	3.92
			3.92
$Y_3O_5^-$	X	24a'	2.47
(C_s $^1A'$)		13a''	2.60
		23 a'	2.77
$Y_3O_6^-$	X	14 a''	1.97
(C_s $^1A'$)			

[a] The labels α and β denote majority and minority spins, whereas D and Q denote doublet and quartet Y_3O_3 final states upon photodetachment, respectively.

[b] The labels denote the peaks in the simulated PES.

Structural Evolution, Sequential Oxidation and Chemical Bonding in Tri-yttrium Oxide Clusters: $Y_3O_x^-$ and Y_3O_x (x = 0–6)

Lei Xu[a], Chan-Juan Xia[a], Ling-Fei Wang[a], Lu Xie[a], Bin Wang[a], Yong-Fan Zhang[a,b]*, Xin Huang [a,b]*

Table of contents entry

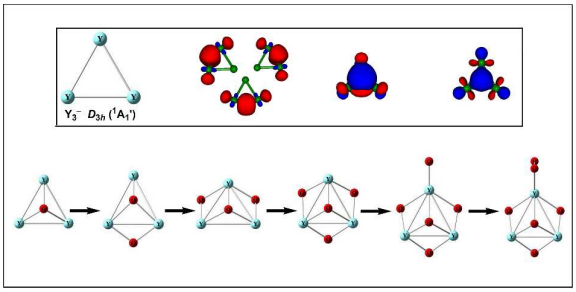

The evolutive regularities for $Y_3O_x^{-/0}$ (x = 0–6) and all-metal aromaticity of Y_3^- cluster have been discovered, respectively.